Revista Mexicana de Astronomía y Astrofísica, **59**, 67–82 (2023)

https://doi.org/10.22201/ia.01851101p.2023.59.01.04

PHOTOMETRIC OBSERVATIONS OF MINOR PLANETS WITH THE TONANTZINTLA SCHMIDT CAMERA I. LIGHT CURVE ANALYSIS OF MAIN-BELT AND NEAR-EARTH ASTEROIDS

J. R. Valdés[1], R. Mújica[1], J. Guichard[1,2], S. Camacho[1,2], G. Cerdán[1], J. Michimani[1], and R. Vega[1]

Received April 28 2022; accepted September 15 2022

ABSTRACT

We report photometric observations of nine main-belt asteroids (MBAs), four near-Earth asteroids (NEAs), and one Mars-crossing asteroid (MCA) carried out with the historical Tonantzintla Schmidt Camera between 2015 and 2018, as part of a process of reactivation of this telescope for astrometric and photometric follow-up observations of MBAs and NEAs. This observational program is part of the commitment made by INAOE when requesting its inclusion in the International Asteroid Warning Network (IAWN). We present the light curves of these 14 asteroids and their corresponding Fourier analyses to determine the rotation period of the asteroids and the brightness amplitude of their light curves.

RESUMEN

Reportamos las observaciones fotométricas de nueve asteroides del cinturón principal (MBAs), un asteroide que cruza la órbita de Marte (MCA) y cuatro asteroides cercanos a la Tierra (NEAs), realizadas con la histórica Cámara Schmidt de Tonantzintla, entre 2015 y 2018, como parte de un proceso de reactivación de este telescopio para dedicarlo a observaciones astrométricas y fotométricas de MBAs y NEAs. Este programa observacional forma parte de las tareas que el Instituto Nacional de Astrofísica, Óptica y Electrónica (INAOE) debe llevar a cabo luego de solicitar su inclusión en la Red Internacional de Alerta de Asteroides (IAWN). Presentamos las curvas de luz de estos 14 asteroides y el análisis de Fourier que permitió determinar el periodo de rotación y la amplitud de la variación de la curva de luz.

Key Words: minor planets, asteroids: general — techniques: photometric

1. INTRODUCTION

Photometric observations of asteroids are very useful due to rapid variations of the observed geometry, even during one opposition. A good average of these geometries can produce a robust physical model of the asteroid that describes its state of rotation and global shape (Kaasalainen et al. 2002). Physical properties such as the rotation period, the amplitude of the light curve (the ratio between two asteroid axes, one side-on and one point-on), the absolute magnitude, H, and the slope parameter, G, are obtained from the photometric observations. To calculate the last two parameters, we need to know, in addition, the distance of the asteroid from the Earth and the Sun at the time of the observations. The first two parameters are obtained from the analysis of the light curve. Applying the inversion method to the light curves observed at different phase angles, and from at least two different oppositions (Kaasalainen & Torppa 2001; Kaasalainen et al. 2001, 2004) allows us to obtain physical parameters, such as the inclination of the rotation axis, the size and the shape of the asteroids, in a reliable manner.

In the last decades, the introduction of CCD detectors made possible a remarkable increase in the number of asteroids for which their state of rotation is known. The large amount of accumulated data has established clear patterns in the rotation of small bodies of the Solar System, and in particular,

[1]Instituto Nacional de Astrofísica, Óptica y Electrónica (INAOE), Puebla, México.
[2]Centro Regional de Enseñanza de Ciencia y Tecnología del Espacio para América Latina y el Caribe (CRECTEALC), México.

the fact that the small asteroids have short periods of rotation (Pravec & Harris 2000). The large population of NEAs discovered in recent years has also made possible the study of small asteroids that are very fast rotators.

The observations reported here are part of an extended program that we started in 2015 with two main goals. First, to contribute to the determination of physical parameters of MBAs and NEAs within the framework of the participation of the Mexico Campus of the Regional Centre for Space Science and Technology Education for Latin America and the Caribbean (CRECTEALC) and the INAOE Astrophysical Department in the activities of the International Asteroid Warning Network (IAWN); and secondly, to reactivate the Tonantzintla Schmidt Camera (CST) as a full-time telescope for astrometric and photometric observations of minor bodies of the Solar System.

The paper is organised as follows: in § 2 we describe the CST status, in § 3 we discuss the observational strategy and data reduction procedure. How we obtained the composite light curve of the observed asteroids and the results of the Fourier analysis for each object are presented in § 4 and § 5, respectively. At the end, we present our perspectives and conclusions.

2. REACTIVATION OF THE TONANTZINTLA SCHMIDT CAMERA

The fundamental aim of the most recent upgrade of the CST is to use it on a dedicated basis to observe MBAs, NEOs, Potentially Hazardous Asteroids (PHAs, asteroids with a minimum orbit intersection distance to Earth's orbit equal or less than 0.05 AU and an absolute magnitude (H) equal to or less than 22.0), and asteroids that could be targets of future space missions. Astrometric and photometric observations were carried out to determine precise orbital parameters of asteroids belonging to the aforementioned groups that permitted us to determine other parameters such as rotation periods, shapes, sizes and inclination of the axes of rotation.

The CST introduced Mexico into modern astrophysics. In the 1940s, the CST was one of the most important telescopes of its class in the world, due to the size of its mirror (D = 77.4 cm), as well as its location, at a latitude of 19° N, in the National Astrophysical Observatory of Tonantzintla (OANTon), in Puebla, Mexico. The CST made it possible to observe the entire plane of the Galaxy, something that was not possible from other observatories in the northern hemisphere. The optical system was built in the Harvard Observatory workshops. The telescope started operation in 1944, but its main scientific observations were carried out between 1948 and 1994. During this period, the CST telescope produced a vast collection of direct (10,446 photographic plates) and spectroscopic images (4,236 photographic plates); the latter were acquired through a 3.96° and 69.85 cm diameter objective prism. The spectroscopic plates had a primary astrophysical value, covering a 10° strip of the entire galactic disk, the galactic center, the galactic poles, and the regions of the M31 and M33 galaxies (Díaz-Hernández et al. 2011). This plate collection is now part of the UNESCO Memory of the World-Mexico.

Since 1948, under the guidance of Guillermo Haro, the CST was dedicated to the development of a series of strategic research lines, among which we can mention the observation of planetary nebulae, Herbig-Haro objects, T-Tauri stars, flare stars, young stars in the direction of the galactic poles, blue emission line galaxies, quasars and the spectral classification of stars, mainly in the southern region of the celestial sphere. Most of the scientific results derived from these investigations were published in the Bulletin of the Tonantzintla and Tacubaya Observatories (1952-1973).

Due to the light pollution caused by the growth of the cities around the OANTon and the low quantum efficiency of the astronomical plates, as of the mid-1990s these detectors were no longer used in astronomical observations with the CST. A new image acquisition system was installed, using a cooled CCD detector, a field flattening lens, and a new telescope control system (Jáuregui-García et al. 2014). In 2015, a new telescope upgrade was done. This included recoating of the reflecting surface of the mirror, cleaning of the corrector lens, maintenance of the mechanical system of the telescope and renewal of the electronic data acquisition system (Valdés et al. 2015a,b). As mentioned, the current CST optical system has an additional component, a field flattening lens. Using direct images taken with the CST in its current configuration, we empirically calculated the image scale of the optical system and obtained a value of 96.6 arcsec/mm, which coincides with the results reported by Cardona et al. (2011).

It is known that in 1945 the CST mirror was returned to the Harvard Observatory to be rectified; however, the results of this correction were never published. Because of this, one of the objectives of the 2015 upgrade was to determine the true focal length (F) of the mirror using a Ronchi interferometric test, which gave a result of $F = 2158.8 \pm 1.4$ mm.

We also used a high precision ION laser tracker to produce a 3D model of the mirror topography using more than 50 contact points on its surface. The high-precision, 3D model obtained made it possible to determine the radius of curvature ($Rc = 4314.8 \pm 0.22$ mm) and the focal length ($F = 2157.4 \pm 0.7$ mm) of the mirror. This value of F produces a plate scale of 95.6 arcsec/mm. Our results contrast with those reported by Wolfschmidt (2009), $F = 2170$ mm and plate scale, $s = 95.05$ arcsec/mm.

In order to verify the results obtained from the optical tests performed on the telescope mirror, a 60.3 × 59.3 arcmin section of an astronomical plate taken with the Schmidt Camera, with central coordinates AR = 07h 18m 42.3s and DEC = $+35^\circ\,42'\,10''.7$, was digitized at a resolution of 1,600 pixels/inch, which produced a pixel of 15.8 microns. The astrometric measurements on the digitized image yielded a plate scale of 1.51 arcsec/pixel. Considering that one pixel equaled 15.8 microns, the plate scale in the digitized image was 95.56 arcsec/mm, which is in good agreement with the plate scale values (95.6 arcsec/mm) calculated from the optical tests. Previously, Díaz-Hernández et al. (2011) had reported a plate scale of 1.51 arcsec/pix in a study performed on the CST spectroscopic plates, providing a dispersion of 1.533 mm between Hβ and Hγ, 0.954 mm between Hγ and Hδ, and 0.626 mm between Hδ and Hϵ.

3. OBSERVATIONAL STRATEGY

3.1. *The Sample*

This observation program was designed in the framework of the commitments acquired by INAOE when requesting its inclusion in the IAWN, an international asteroid warning network under the auspices of the United Nations (UN) and the leadership of the NASA's Planetary Defense Coordination Office (PDCO). IAWN was established in 2014 as a result of recommendations made by the UN General Assembly in 2013 to create an international network of organizations involved in detecting, tracking, and characterizing NEOs, as an international response to a potential NEO impact threat. At the time of writing of this article, IAWN had a membership of 40 observatories. The IAWN is tasked with developing a strategy using well-defined communication plans and protocols to assist governments in the analysis of asteroid impact consequences and in the planning of mitigation responses.

The observed asteroids presented here were selected using the Ephemeris Generator of the Collaborative Asteroid Light Curve Link[3]. From the list of observable asteroids from the CST location, we selected those whose periods are known as they are necessary for shape determination. In addition, we wanted to verify the accuracy of periods as observed by the CST. We chose asteroids with rotational periods between two and three hours that can be covered at least twice per night. Nevertheless, we made some exceptions. We also observed objects with periods that could not be observed completely in one night to see if we could construct the phase plot light curve by observing the object during 2–3 nights. Other selection criteria were the possibility of covering a phase angle variation greater than 20 degrees during the observed opposition and that the orbital velocities should be less than 4.45 arcsec/min in order to keep the asteroid in the same field throughout the night, avoiding the need to change the reference stars used to construct the light curve.

On the other hand, in order to apply the light curve inversion method to determine the asteroid shape, it is necessary that the selected asteroids have publicly available light curves on the Asteroid Light curve Photometry Database (ALCDEF). According to the minor planet Light curve Database (LCDB) file description (Warner et al. 2009), the U code provides an assessment of the quality of the period solution, not necessarily of the data per se. The rating goes from 3, for a completely unambiguous light curve, in terms of the calculated period, to 0 for a result that later was proven to be incorrect. It is therefore desirable that the parameter defining the LCDB Status has values U=3 or 3-, which means that the quality of the light curves is optimal.

The observed set of objects consisted of 14 asteroids: nine main-belt asteroids (MBAs), four Near-Earth Asteroids (NEAs), and one Mars-crossing asteroid (MCAs), as listed in Table 1.

3.2. *Observations and Data Reduction*

Photometric observations were carried out with the 77.4 cm Tonantzintla Schmidt Camera of INAOE between October and December 2015 and between March and May 2018. The telescope's current optical system has a field-flattening lens that provides a focal distance of 2135.2 mm and an image scale of 96.6 arcsec mm^{-1}. During the 2015 observing runs we used a 1530 × 1020 pixel (9.0 × 9.0 μm^2) SBIG ST-8 CCD camera, that produced an image scale of 0.86 arcsec pix^{-1}, and a field-of-view (FOV) of 22.2 × 14.8 arcmin.

[3] https://minplanobs.org/MPInfo/php/callopplcdbquery.php

At the beginning of 2018 we upgraded the image acquisition system with the installation of a SBIG STF-8300 color CCD Camera, equipped with a 3326 × 2540 pixel ($5.4 \times 5.4\mu m^2$) high resolution Kodak KAF-8300C full frame sensor with microlens technology and antiblooming for improved quantum efficiency. This new system provides an image scale of 0.52 arcsec pix^{-1}, and a FOV of 28.8×22.0 arcmin.

Selected physical parameters of the observed asteroids, such as semi-major axis (a), eccentricity (e), taxonomic class, absolute magnitude (H), diameter, and albedo, are listed in Table 1, while their observational circumstances, including geocentric (r) and heliocentric (Δ) distances, and phase angle (α), are shown in Table 2. Where there were different albedo values reported for the same asteroid, we gave preference to the Wide-field Infrared Survey Explorer *WISE* measurements (Mainzer et al. 2011).

When the absolute magnitude and the albedo of observed asteroids were known, their diameters were calculated using equation (1), where p_ν is the reported albedo. Otherwise, when there were no reports on the asteroid albedos, we used equation (2), assuming that the average albedo of asteroids is 14% and that an asteroid whose absolute magnitude is 17.75, corresponds to an asteroid of 1 km in size.

$$D = 10^{[6.259 - log_{10} p_\nu - 0.4 \times H]}, \quad (1)$$

$$D = (1\text{km}) \times 10^{(17.75 - H)/5}. \quad (2)$$

Depending on the brightness of the observed objects and weather conditions, the integration times varied between 30 and 120 s. For each observing run, master bias, dark and flat-field images were produced. Scientific images were corrected for bias, dark and flat-field effects using Image Reduction and Analysis Facility (IRAF) packages.

Differential photometry and period analysis were done using the *MPO Canopus* analysis tool (Warner 2014). In each case, we used four solar analogs nonvariable comparison stars, in the same FOV, to generate light curves. Comparison stars were selected near the path covered by the asteroids during the night.

4. LIGHT CURVE ANALYSIS

The obtained light curves for the observed asteroids are presented in Figures 1 to 14, and the results of the corresponding Fourier analysis (Harris et al. 1989) in Table 3. Assuming that the light curve of an asteroid is produced by a given geometry in rotation, the brightness of an object is proportional to the projected area, and the ratio of minimum to maximum cross sections (CS_{min}, and CS_{max}, respectively) is determined by the peak-to-peak amplitude (A) of the light curve through a very simple formula (Harris et al. 2014):

$$A = -2.5 \log(CS_{min}/CS_{max}). \quad (3)$$

This ratio, the values of the rotation period, and the amplitude of the light curve, are reported in Table 3. In order to resolve the possible ambiguities in deriving the correct rotation periods of observed asteroids, we used the constraints on amplitude variation *versus* harmonic order of the Fourier function proposed by Harris et al. (2014). The Fourier fit order used in the composite light curve is shown in the fifth column of Table 3.

The light curves show the relative instrumental magnitude *versus* the rotational phase, calculated with the rotation periods given in Table 3. The caption of the figures indicates, for each night, the plot symbol used, the UT time of observations, the JD for zero rotational phase, and the corresponding phase angle. The zero phase is corrected for the light travel-time effect. Uncertainty bars are plotted for each individual data point. The *MPO Canopus* Fourier analysis tool provides the period solution and the Fourier coefficients defining the shape of the composite light curve for each data set. The solution also provides the instrumental magnitude offset between each asteroid and its comparison stars, for each individual light curve that we used to calculate the peak-to-peak amplitude of the composite light curves.

5. RESULTS

5.1. *(711) Marmulla*

(711) Marmulla (1911 LN, 1927 AB) is an Inner Main-Belt asteroid, that belongs to the Flora family (a = 2.2369 AU., i = 6.0991°). It was discovered on March 1, 1911 by J. Palisa at Vienna. (711) Marmulla has albedo values that correspond to a S-class asteroid; $p_V = 0.22 \pm 0.09$ (Nugent et al. 2016), and $p_V = 0.224 \pm 0.030$ (Usui et al. 2011).

We observed this asteroid at four different values of phase angle, $\alpha = 7.68°$, 9.52° (grouped in a single light curve), 12.95°, and 22.11°. We obtained 37 images on March 12, 2018, 187 images on March 16, 2018, 109 images on March 24, and 88 images on April 9, 2018; exposure times ranged from 50 to 90 s.

The best values for the periods obtained from the Fourier analysis of our three light curves

TABLE 1

SELECTED PHYSICAL PARAMETERS OF THE OBSERVED ASTEROIDS

Asteroid	a (AU)	e	Taxonomic class	H (mag)	Diameter (km)	Albedo	Comments
(711) Marmulla	2.2369	0.1955	S, Sr	11.84	12.31	0.22±0.09[a]	MB-Inner Asteroid Flora family
(1036) Ganymed	2.6629	0.5335	S,Sr	9.25	40.76	0.218±0.048[b]	NEA, Amor group
(1117) Reginita	2.2475	0.1983	S	11.81	9.77	0.3585±0.0785[b]	MB-Inner Asteroid
(1318) Nerina	2.3073	0.2039	M	12.37	10.90	0.1721±0.0208[b]	MB-Inner Asteroid Phocaea family
(1346) Gotha	2.6269	0.1782	S	11.44	13.13	0.2794±0.0411[b]	MB-Middle Asteroid Eunomia family
(1363) Herberta	2.9036	0.0682	S	11.36	12.4	0.337±0.157[c,d]	MB-Outer Asteroid Koronis family
(1492) Oppolzer	2.1729	0.1165	S	13.0	11.34	0.089±0.026[e]	MB-Inner Asteroid
(1627) Ivar	1.8630	0.3965	S,Sr	12.68	10.71	0.134±0.025[b]	NEA, Amor group
(1831) Nicholson	2.2390	0.1279	S	12.57	7.58	0.296±0.053[c,d]	MB-Inner Asteroid
(1847) Stobbe	2.6114	0.0214	Xc,M	11.13	16.64	0.2315±0.0162[b]	MB-Middle Asteroid
(1866) Sisyphus	1.8933	0.5384	S,Sw	12.44	8.67	0.255±0.0162[b]	NEA, Apollo group
(3800) Karayusuf	1.5779	0.0757	S	15.09	1.59	0.657±0.123[d,f]	Mars-crosser
(5692) Shirao	2.6554	0.1819	S	12.55	8.84	0.2218±0.0290[b]	MB-Middle Asteroid
(25916) 2001 CP44	2.5613	0.4979	Sw	13.68	4.83	0.262±0.047[b]	NEA, Amor group

[a]Nugent et al. (2016). [b]Mainzer et al. (2011). [c]Masiero et al. (2012). [d]Mainzer et al. (2016). [e]Tedesco et al. (2004). [f]Nugent et al. (2015).

(2.804±0.001 h, 2.876±0.074 h, and 2.627±0.041 h) are very similar to the values on the LCDB database reported by different authors.

5.2. *(1036) Ganymed*

Asteroid (1036) Ganymed is the largest NEA that we observed. It belongs to the Amor group, and is classified as S type with an albedo of 0.218±0.048 (Mainzer et al. 2011) and a corresponding diameter of 40.76 km. It was discovered by W. Baade at the Bergedorf Observatory in Hamburg on 23 October, 1924.

We observed this asteroid at three different values of phase angle, $\alpha = 6.18°$, 6.26° and 6.35°. Observations are grouped in a single light curve. We obtained 382 images on March 19, 2018, with an exposure time of 40 seconds, and 653 images on March 20, 2018, and 276 images on March 21, 2018, with exposure times of 30 s.

From the Fourier analysis of the light curve we show here, we obtained a value of the period equal to 10.318±0.013 h, very similar to the 35 values compiled on LCDB.

5.3. *(1117) Reginita*

(1117) Reginita (1927 KA) is an Inner Main-Belt asteroid. It was discovered on May 24, 1927 by J. Comas Solú at the Fabra Observatory in Barcelona (Schmadel 2012). (1117) Reginita has a very high albedo among the taxonomic class S. Pravec et al. (2012) reported a value of $p_V = 0.3516$ from *WISE* thermal observations while Nugent et al. (2016) obtained an albedo of 0.36±0.13, and a diameter D=9.82±2.35 km from *NEOWISE* Reactivation Mission observations. Mainzer et al. (2011) derived $p_V = 0.3585 \pm 0.0785$, and D=10.193±0.250 km applying thermal models to the *NEOWISE* data at 3.4, 4.6, 12, and 22 μm.

On October 4, 2015, at a phase angle of 16.73°, we obtained 221 images with a 30 s exposure time. Fourier analysis of the light curve produced the best fit at 2.942±0.012 h, similar to the values reported by Wisniewski, Michalowski & Harris (1995), Kryszczyńska et al. (2012), Chang et al. (2015), Waszczak et al. (2015), and another seven authors included on LCDB. The obtained peak-to-peak amplitude, 0.16 magnitude, is in the range of values reported by the previously mentioned authors for this asteroid. We observed again Reginita in 2018, obtaining almost the same result 2.945±0.002 h, by using 81 images of 60 s exposure time at a phase angle of 22.70°, obtained on April 8, and 74 images

TABLE 2

OBSERVATIONAL CIRCUMSTANCES FOR THE OBSERVED ASTEROIDS

Asteroid	Date (UT)	RA (J2000.0)	DEC (J2000.0)	Δ (AU)	r (AU)	α (degrees)	V (mag)	Filter[a]
(711) Marmulla	2018 Mar. 12.67	10h 19m 48.2s	+13° 36′ 59″.5	1.5590	2.5180	7.68	15.2	C
	2018 Mar. 16.66	10h 15m 53.5s	+13° 47′ 24″.7	1.5727	2.5112	9.52	15.3	C
	2018 Mar. 24.69	10h 09m 00.9s	+14° 01′ 28″.8	1.6102	2.4985	12.95	15.5	R
	2018 Apr. 09.63	10h 00m 32.1s	+14° 00′ 05″.9	1.4824	2.2052	22.11	16.0	R
(1036) Ganymed	2018 Mar. 19.10	10h 43m 02.0s	−18° 54′ 38″.0	3.1662	4.0832	6.21	15.4	C
	2018 Mar. 20.10	10h 42m 18.7s	−18° 46′ 40″.0	3.1682	4.0834	6.22	15.4	C
	2018 Mar. 21.20	10h 41m 31.5s	−18° 37′ 42″.0	3.1701	4.0835	6.23	15.4	C
(1117) Reginita	2015 Oct. 04.10	23h 04m 02.6s	−10° 28′ 14″.0	1.013	1.956	13.73	14.0	C
	2018 Apr. 08.85	16h 34m 57.2s	−14° 58′ 38″.2	1.2511	2.0314	22.70	14.8	R
	2018 Apr. 09.63	10h 00m 32.1s	−14° 00′ 05″.9	1.2435	2.0298	22.51	14.8	R
(1318) Nerina	2018 Mar. 17.59	11h 19m 14.5s	+11° 38′ 33″.6	0.0879	1.8634	6.52	13.7	R
	2018 Mar. 27.56	11h 02m 43.1s	+09° 13′ 53″.3	0.0895	1.8547	12.27	14.0	R
(1346) Gotha	2018 Mar. 29.58	07h 12m 43.1s	+12° 59′ 32″.2	2.0593	2.4323	23.88	15.9	R
(1363) Herberta	2015 Dec. 15.01	04h 08m 52.7s	+20° 01′ 38″.0	1.996	2.945	6.18	15.6	C
	2015 Dec. 16.07	04h 08m 05.0s	+19° 59′ 23″.0	2.001	2.945	6.54	15.6	C
	2015 Dec. 17.08	04h 07m 18.7s	+19° 57′ 11″.0	2.007	2.946	6.94	15.7	R
(1492) Oppolzer	2018 Mar. 18.60	11h 26m 34.2s	+11° 06′ 23″.4	0.9991	1.9840	5.85	14.8	R
	2018 Mar. 26.59	11h 19m 46.2s	+12° 14′ 25″.1	1.0114	1.9763	10.27	15.0	R
(1627) Ivar	2018 Mar. 17.26	15h 08m 07.2s	−02° 07′ 19″.0	0.8931	1.7084	26.71	14.8	C
	2018 Mar. 27.23	15h 15m 17.8s	−00° 19′ 43″.0	0.7784	1.6543	24.37	14.4	R
(1831) Nicholson	2018 Mar. 10.79	10h 11m 31.8s	+21° 32′ 15″.5	1.3065	2.2495	10.42	15.4	C
	2018 Mar. 11.62	10h 10m 44.6s	+21° 35′ 12″.3	1.3095	2.2481	10.89	15.4	C
	2018 Mar. 14.67	10h 11m 31.8s	+21° 32′ 15″.5	1.3065	2.2495	10.42	15.4	C
	2018 Mar. 25.59	10h 00m 07.4s	+21° 58′ 48″.7	1.3748	2.2275	17.00	15.7	R
	2018 Apr. 14.58	09h 55m 39.8s	+21° 15′ 25″.6	1.5245	2.1978	23.43	16.1	R
	2018 Apr. 20.61	09h 56m 55.2s	+20° 47′ 35″.0	1.5781	2.1889	24.78	16.2	R
	2018 Apr. 21.60	09h 57m 14.3s	+20° 42′ 24″.9	1.5872	2.1874	24.98	16.2	R
(1847) Stobbe	2018 Abr. 18.71	15h 20m 07.8s	−01° 26′ 49″.7	1.6289	2.5612	9.77	14.9	R
(1866) Sisyphus	2018 Mar. 25.32	13h 26m 02.8s	+53° 01′ 21″.0	2.2221	2.8935	16.72	17.3	C
(3800) Karayusuf	2018 Mar. 28.79	15h 59m 16.6s	+14° 15′ 06″.1	0.6393	1.4596	34.23	16.3	R
(5692) Shirao	2018 Mar. 18.80	12h 44m 30.8s	−03° 20′ 21″.6	1.2770	2.2558	6.22	15.1	R
	2018 Mar. 26.79	12h 39m 24.5s	−01° 46′ 18″.8	1.2505	2.2459	2.21	14.8	R
	2015 Apr. 07.74	124h 31m 10.7s	+00° 37′ 20″.9	1.2411	2.2321	4.86	14.9	R
(25916) 2001 CP44	2018 Apr. 14.36	16h 41m 45.5s	+03° 31′ 27″.0	0.8411	1.6754	27.21	15.6	R
	2018 Apr. 16.33	16h 43m 19.0s	+03° 39′ 11″.0	0.8193	1.6632	26.92	15.5	R

[a]C = Clear filter (no filter), R = R-band filter.

of 90 s exposure time, at a phase angle of 22.43°, obtained on April 9.

5.4. *(1318) Nerina*

(1318) Nerina is an inner Main-Belt asteroid, belonging to the Phocaea family. It was discovered on March 24, 1934 by C. Jackson at Johannesburg (Schmadel 2012). Mainzer et al. (2011) derived a value of $p_V = 0.1721 \pm 0.208$ that is in correspondence with an M-type asteroid.

We observed (1318) Nerina at two values of phase angle, $\alpha = 6.52°$, and 12.27°. We obtained 377 images with 30 s exposure time on March 17, 2018, and 84 images on March 27, 2018, with a 60 s exposure time.

The Fourier analysis of the two light curve data we obtained gave us the period values 2.586±0.013 h and 2.463±0.033 h, both with a difference of less than one percent with respect to the 11 values found on the LCDB database.

TABLE 3

ROTATION PERIOD AND BRIGHTNESS AMPLITUDE OF THE OBSERVED ASTEROIDS

Asteroid	Period* (h)	Period** (h)	Amplitude (mag)	Fourier fit order	CS_{min}/CS_{max}
(711) Marmulla	2.804±0.001	2.721	0.13	8th	0.89
	2.876±0.074		0.09	6th	0.92
	2.627±0.041		0.17	6th	0.86
(1036) Ganymed	10.318±0.013	10.297	0.15	6th	0.87
(1117) Reginita	2.944±0.012	2.946	0.16	4th	0.86
	2.945±0.002		0.28	6th	0.77
(1318) Nerina	2.586±0.013	2.528	0.07	6th	0.94
	2.463±0.033		0.10	8th	0.91
(1346) Gotha	2.563±0.057	2.64067	0.21	6th	0.82
(1363) Herberta	3.018±0.002	3.015	0.16	8th	0.86
(1492) Oppolzer	3.770±0.020	3.76945	0.11	8th	0.90
	3.566±0.076		0.11	8th	0.90
(1627) Ivar	4.795±0.001	4.795	0.90	2nd	0.44
(1831) Nicholson	3.216±0.001	3.228	0.29	8th	0.77
	3.220±0.022		0.31	6th	0.75
	3.217±0.001		0.41	8th	0.69
(1847) Stobbe	5.621±0.012	5.617	0.41	6th	0.61
(1866) Sisyphus	2.391±0.028	2.400	0.12	6th	0.91
(3800) Karayusuf	2.270±0.084	2.2319	0.32	4th	0.74
(5692) Shirao	2.957±0.032	2.8878	0.13	6th	0.89
	2.900±0.055		0.13	4th	0.89
	2.866±0.085		0.14	6th	0.88
(25916) 2001 CP44	4.2020±0.0024	4.6021	0.22	6th	0.82

*The value derived in this work.
**The value in the LCDB summary table.

5.5. *(1346) Gotha*

(1346) Gotha is a Main-Belt asteroid that belongs to the Eunomia family. It was discovered in 1929, on February 5, by K. Reinmuth at Heidelberg (Schmadel 2012). Mainzer et al. (2011) derived a value of $p_V = 0.2794 \pm 0.0411$, in agreement with a S-type taxonomic classification established by Tholen (1984).

From the light curve generated with 62 images of 120 s exposure time obtained on March 29, 2018, at a phase angle α equal to 23.88°, the best fit value obtained for the period, from the Fourier analysis, is 2.563±0.057 h, consistent with five out the six values reported on the LCDB database.

5.6. *(1363) Herberta*

(1363) Herberta (1935 RA) is an Outer Main-Belt asteroid, belonging to the Konoris family ($2.83 < a < 2.91$, $i < 3.5$). It was discovered on August 30, 1935 by E. Delporte at the Royal Belgium Observatory in Uccle (Schmadel 2012). Based on MOVIS NIR colors, Popescu et al. (2018) proposed a S-type taxonomic classification. The value of albedo $p_V = 0.337 \pm 0.157$, determined by Masiero et al. (2012), is close to the upper limit for S-complex asteroids.

A total of 427 images of Herberta were taken over three nights, from December 15 to 17, 2015 with 60 s of exposure time. The phase angle values for the observation nights were 6.18°, 6.56° and 6.94°, respectively. All the observations were grouped in a single light curve.

The best value we obtained for the period, from the Fourier analysis, is equal to 3.018±0.002 h; meanwhile, the only value reported on LCDB is equal to 3.015±0.005 h.

5.7. *(1492) Oppolzer*

(1492) Oppolzer was discovered in 1938 by Y. Väisälä (Schmadel 2012). (1492) Oppolzer is a S-type (Vereš et al. 2015) Inner Main-Belt asteroid. The taxonomy for this asteroid was determined from

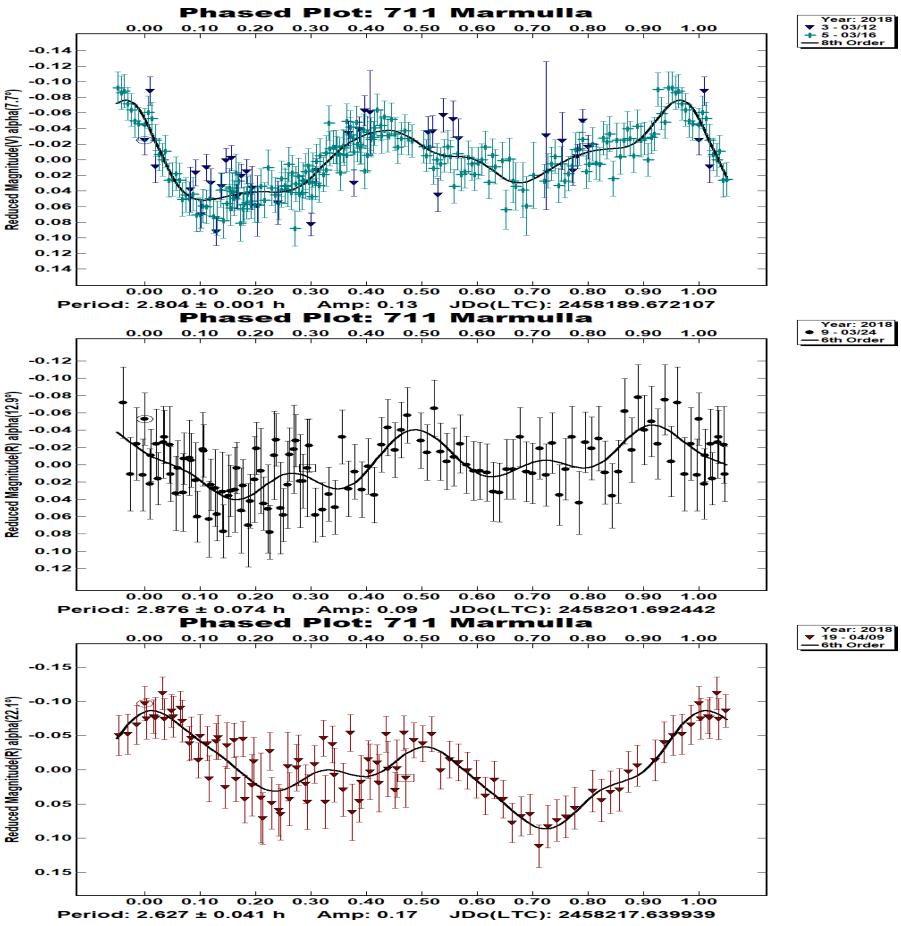

Fig. 1. Light curves of (711) Marmulla observed on March 12, 16 and 24, and April 9, 2018. The color figure can be viewed online.

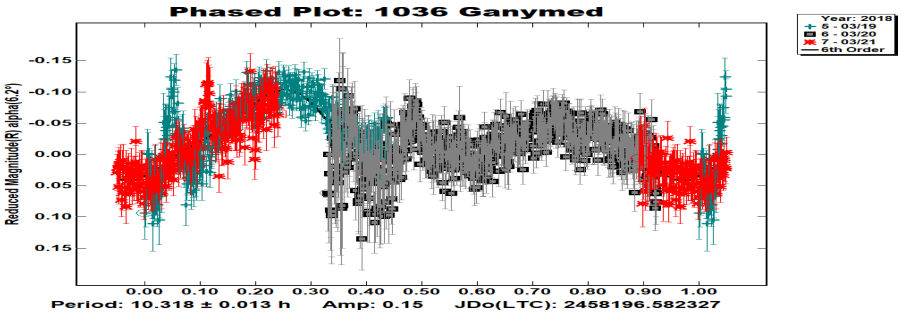

Fig. 2. Composite light curve of (1036) Ganymed observed on March 19, 20 and 21, 2018. The color figure can be viewed online.

photometry obtained at the Pan-STARRS PS1 telescope; however, the albedo ($p_V = 0.089 \pm 0.026$) reported by Tedesco et al. (2004), using the observations of the *IRAS* mission, is very low and corresponds more closely to a C-class asteroid.

We observed this asteroid at two values of phase angle, $\alpha = 5.85°$ and $\alpha = 10.27°$. We obtained 375 images of 40 s exposure time on March 18, 2018, and 129 images on March 26, 2018, of 60 s exposure time. One of the values we obtained for the period, 3.77±0.02 h, is in complete agreement with the seven values on LCDB, with a difference of less than 0.1 percent. For the second value, 3.566±0.076 h, the difference is larger.

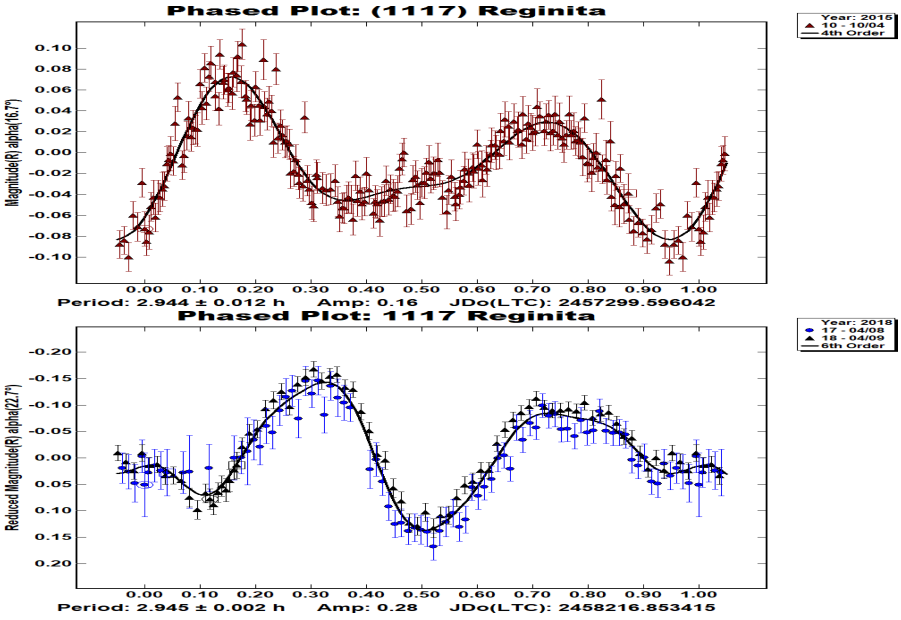

Fig. 3. Top panel: Light curve of (1117) Reginita observed on October 4, 2015. Bottom panel: Light curve of (1117) Reginita observed on April 8 and 9, 2018. The color figure can be viewed online.

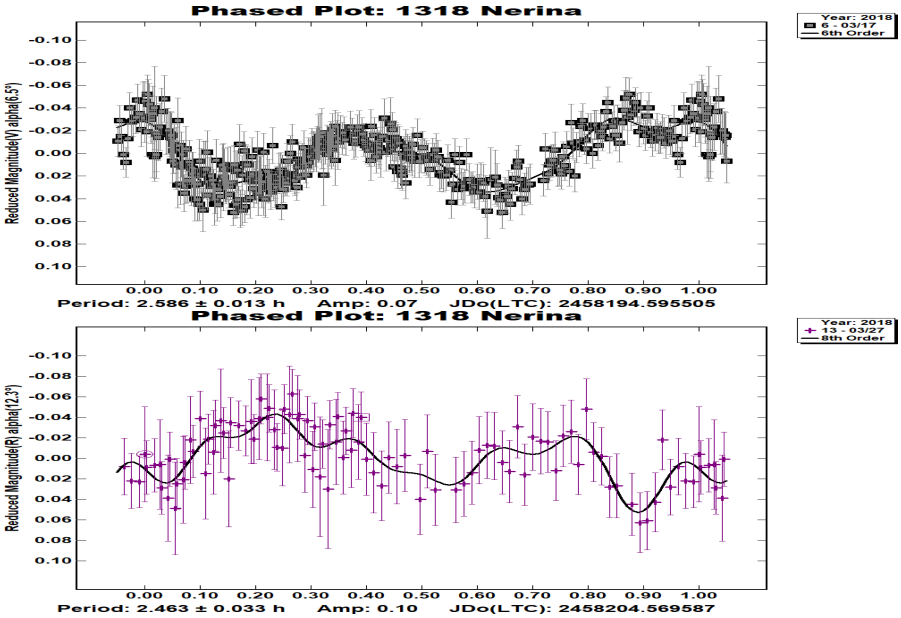

Fig. 4. Top panel: Light curve of (1318) Nerina observed on March 17, 2018. Bottom panel: Light curve observed on March 27. The color figure can be viewed online.

5.8. *(1627) Ivar*

(1627) Ivar was discovered on September 25, 1929 by E. Hertzsprung at Johannesburg (Schmadel 2012).

We obtained 600 images of 30 s exposure time for this asteroid on March 17, 2018, at phase angle $\alpha = 26.71°$, and 68 images of 60 s exposure time on March 27, 2018, at phase angle, 24.33°. As the

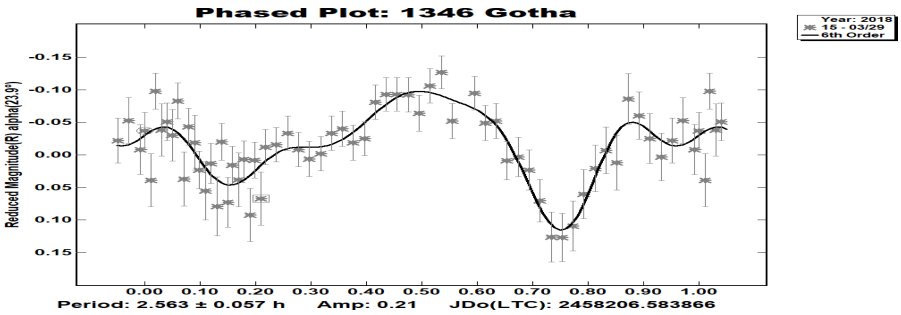

Fig. 5. Light curve of (1346) Gotha observed on March 29, 2018. The color figure can be viewed online.

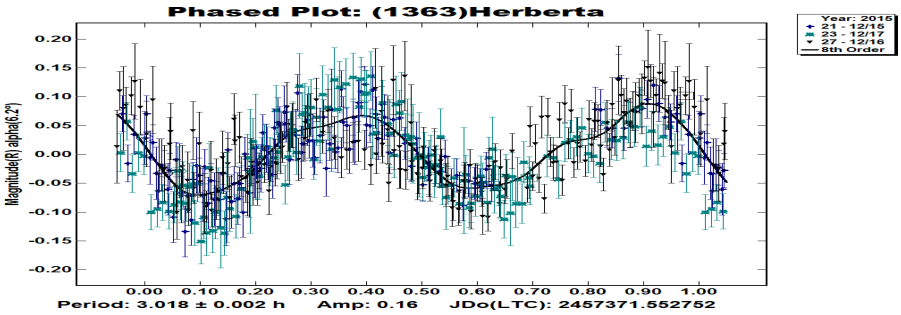

Fig. 6. Composite light curve of (1363) Herberta observed on December 15, 16, 17, 2015. The color figure can be viewed online.

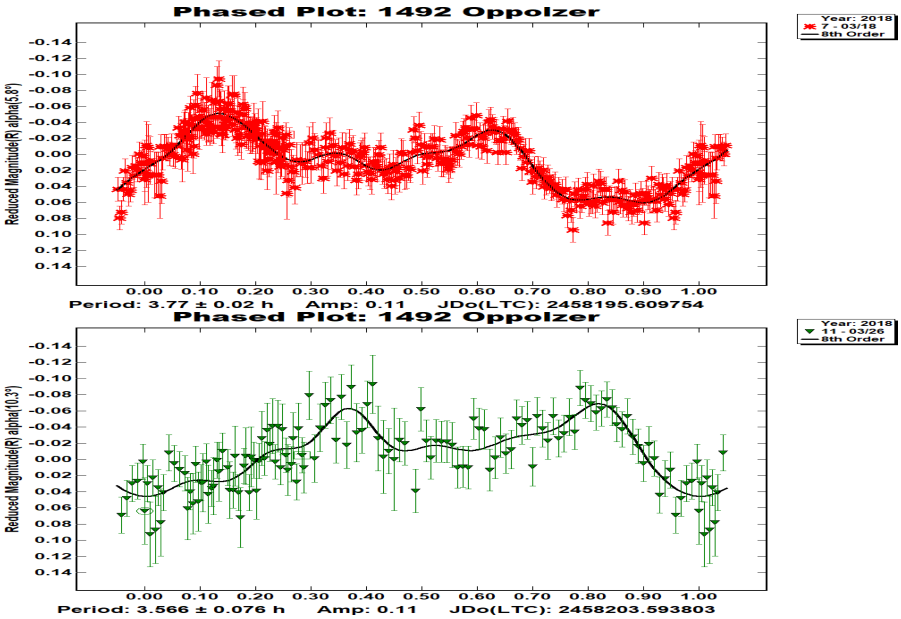

Fig. 7. Top panel: Light curve of (1492) Oppolzer observed on March 18, 2018. Bottom panel: Light curve of (1492) Oppolzer observed on March 26, 2018. The color figure can be viewed online.

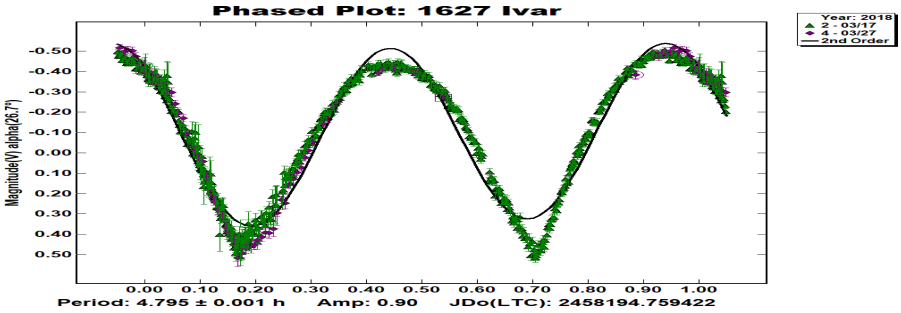

Fig. 8. Composite light curve of (1627) Ivar observed on March 17, 27. 2018. The color figure can be viewed online.

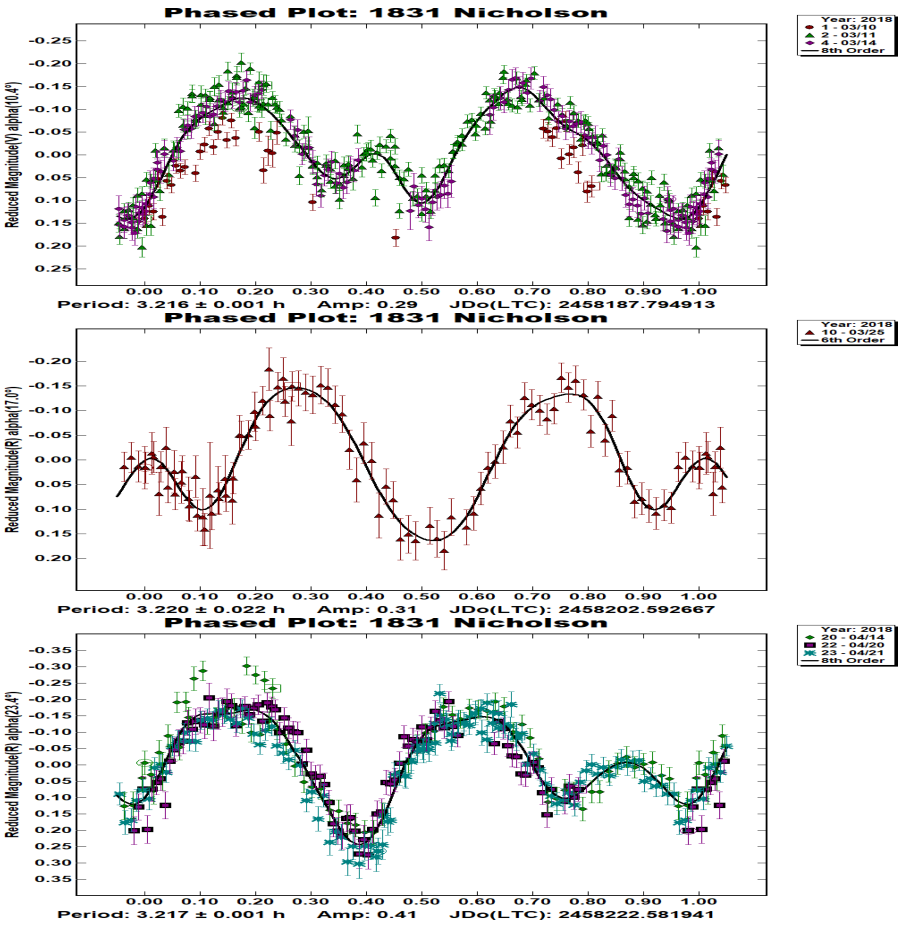

Fig. 9. Top panel: Composite light curve of (1831) Nicholson observed on March 10, 11, 14, 2018. Middle panel: Light curve of (1831) Nicholson observed on March 25, 2018. Bottom panel: Composite light curve of (1831) Nicholson observed on April 14, 20, 21, 2018. The color figure can be viewed online.

phase angles have very similar values, we grouped the observations in a single light curve.

The value we obtained for the period, 4.795±0.001 h is exactly the same as the best value reported on LCDB. This asteroid has been well observed; there are 16 values reported on this database.

5.9. *(1831) Nicholson*

(1831) Nicholson was discovered on April 17, 1968, by P. Wild at Zimmerwald, Switzerland

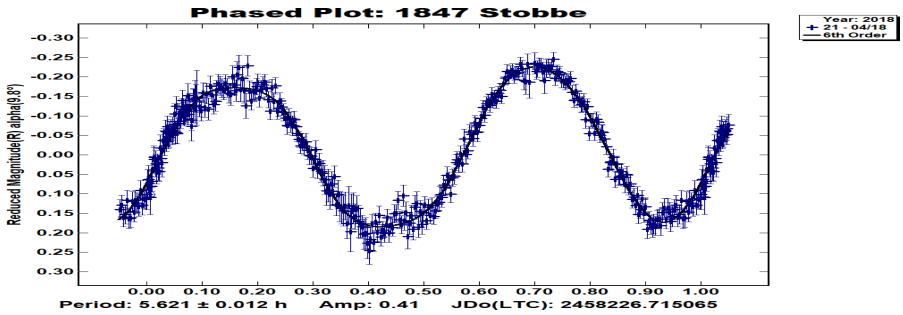

Fig. 10. Light curve of (1847) Stobbe observed on April 18, 2018. The color figure can be viewed online.

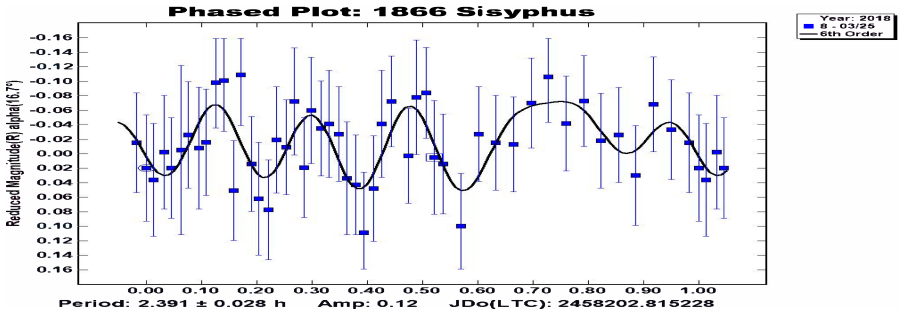

Fig. 11. Light curve of (1866) Sisyphus observed on March 25, 2018. The color figure can be viewed online.

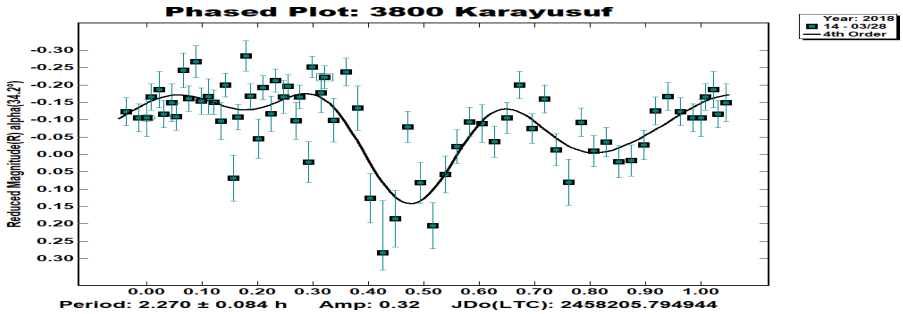

Fig. 12. Light curve of (3800) Karayusuf observed on March 28, 2018. The color figure can be viewed online.

(Schmadel 2012). It is an S-type asteroid (Bus & Binzel 2002) from the inner region of the Main-Belt. Masiero et al. (2012) has estimated an albedo value of $p_V = 0.296 \pm 0.053$ which is in good agreement with the values for S-complex asteroids.

We observed this asteroid in 2018. We grouped the March 10, 11 and 14 observations in a single light curve, the March 25 observations in another, and in a third light curve we grouped observations carried out on April 14, 20 and 21. We obtained 756 images with exposure times ranging from 30 s to 120 s. The phase angles covered were $\alpha = 10.40°$ to $24.98°$.

The best period values obtained from the Fourier analysis for our three light curves, 3.216±0.001 h, 3.220±0.022 h, and 3.217±0.001 h, are completely consistent with the four values on LCDB.

5.10. *(1847) Stobbe*

(1847) Stobbe was discovered on 1916 February 1, by H. Thiele at Bergedorf, Germany (Schmadel 2012). This is a middle Main-Belt asteroid that was originally classified as a Xc asteroid by Bus & Binzel (2002) during the Phase II of the Small Main-Belt Asteroid Spectroscopic Survey. More recently, Mainzer et al. (2011), using NEOWISE photome-

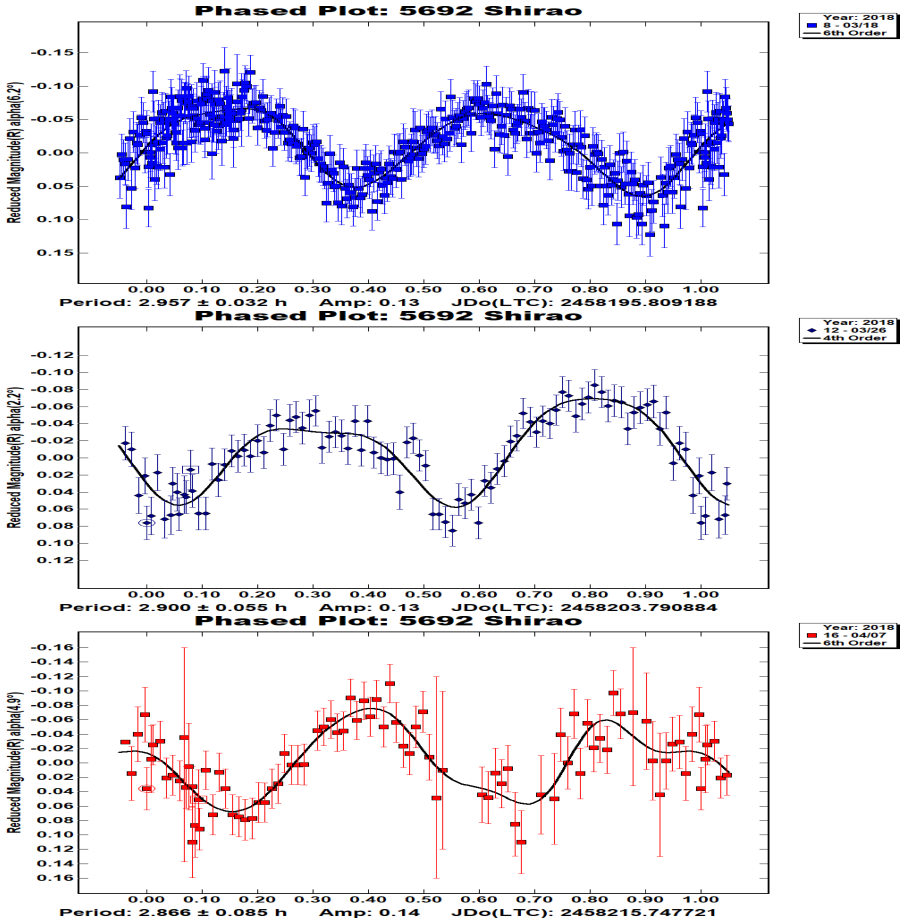

Fig. 13. Top panel: Light curve of (5692) Shirao observed on March 18, 2018. Middle panel: Light curve of (5692) Shirao observed on March 26, 2018. Bottom panel: Light curve of (5692) Shirao observed on April 7, 2018. The color figure can be viewed online.

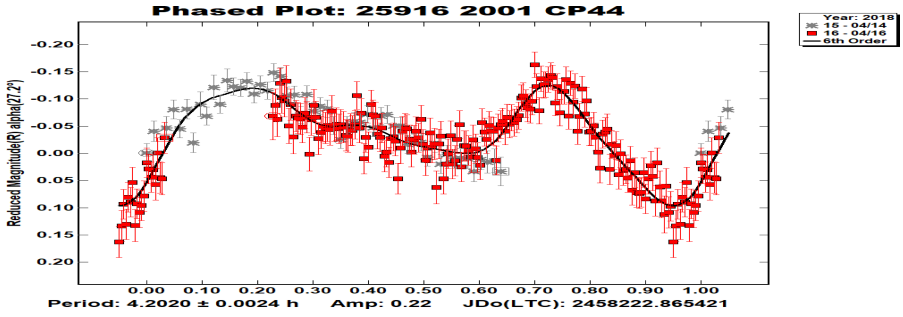

Fig. 14. Composite light curve of (25916) 2001 CP44 observed on April 14, 16, 2018. The color figure can be viewed online.

try, suggested an M-type taxonomy for this asteroid. P-type, M-type and E-type asteroids are included in the larger X-type group and are differentiated by optical albedo values (Tholen & Barucci 1989).

The typical optical albedo for M-type asteroids is between 0.1 and 0.3, so the albedo of $p_V = 0.2315 \pm 0.0162$ reported by Mainzer et al. (2011) corresponds to this type.

We observed this asteroid on April 18, 2018. We obtained 52 images with 60 s exposure time at a phase angle $\alpha = 9.77°$. The period we obtained from the light curve Fourier analysis is equal to

5.621±0.012 h, very similar to three out of the four values on LCDB. The largest difference with our result corresponds to the value 6.37±0.02 (Malcolm 2002), that is also the least recent value obtained.

5.11. *(1866) Sisyphus*

(1866) Sisyphus was discovered on December 5, 1972 by P. Wild at Zimmerwald, Switzerland (Schmadel 2012). It is a NEA that belongs to the Apollo group. Mainzer et al. (2011) reported a value of $p_V = 0.255 \pm 0.049$, which is in correspondence with the taxonomic classifications S-type and Sw-type provided by Bus & Binzel (2002) and Binzel et al. (2019), respectively, both observing this asteroid as part of optical spectroscopic surveys.

This asteroid was observed on March 25, 2018. We obtained 48 images with a 210 s exposure time at a phase angle $\alpha = 16.74°$. Even though the amplitude of this light curve is of a similar order as the photometric uncertainties on the individual points, the best fit we obtained for the period, 2.391±0.028 h, is in agreement with the thirteen values reported on LCDB, most of them around 2.4 h.

5.12. *(3800) Karayusuf*

(3800) Karayusuf is an S-type (Bus & Binzel 2002; Binzel et al. 2019) Mars-crosser (MC) asteroid discovered on January 4, 1984, by E. F. Helin at Palomar in California, USA (Schmadel 2012). A very high value of its albedo, $p_V = 0.66 \pm 0.12$, not corresponding to an S-type asteroid, was reported by Nugent et al. (2015). With an absolute magnitude H=15.09, this albedo value gives a size of 1.59 km, one of the smallest asteroids in our sample. However, Alí-Lagoa & Delbo' (2017), using the NEA thermal model to provide diameters and albedos of MCs with available WISE/NEOWISE data, proposed an albedo $p_V = 0.281 \pm 0.056$ for this asteroid. With this correction, the size of (3800) Karayusuf can increase to 2.43 km.

With an exposure time of 120 s, we obtained 60 images of this asteroid on March 28, 2018. Its phase angle on that night was 34.23° and the derived period was 2.270±0.084 hours. There are 11 values reported on LCDB, all of them quite similar to the one derived from our data.

5.13. *(5692) Shirao*

(5692) Shirao was discovered on March 23, 1992 by K. Endate and K. Watanabe at Kitami (Schmadel 2012). It is an S-type (Vereš et al. 2015) middle Main-Belt asteroid. Mainzer et al. (2011) reported a typical S-type albedo $p_V = 0.2218 \pm 0.0290$.

We observed this asteroid in 2018, on March 18 and 26, and April 7. A total of 235 images were obtained. Exposure time for March 18 images was 30 s and 60 s for the other two nights. The phase angle for March 18 was 6.22°, for March 26 was 2.21° and 4.86° for April 7, so we decided to construct three different light curves. The corresponding periods derived from Fourier analysis are 2.957±0.032 h, 2.900±0.055 h, and 2.866±0.085 h, very similar to the best value reported on the LCDB summary table (2.8878 h).

5.14. *(25916) 2001 CP44*

(25916) 2001 CP44 is the only Amor-type NEA in our sample. It has a diameter of 5.7 km and was discovered by LINEAR at Socorro, New Mexico. This is clearly an S-complex asteroid, classified as an Sq-type (Thomas et al. 2014; Popescu et al. 2019), S-type (Lin et al. 2018), and Sw-type (Binzel et al. 2019). Mainzer et al. (2011) reported a typical S-type albedo $p_V = 0.262 \pm 0.047$.

We obtained a total of 250 images of this asteroid in 2018. On April 14 (53 images, exposure time 120 s, phase angle 27.17°) and April 16 (197 images, exposure time 60 s, and phase angle 26.86°).

From our light curve we derived a period equal to 4.2020±0.0024 h, while, on LCDB there are two clear sets of values, one around 4.2 h, reported during 2012-2014, and another around 4.6 h, reported during 2018. The difference can be due to observations being made during different apparitions.

6. CONCLUSIONS

The results of the analyses of the photometric observations of the 14 asteroids reported in the present work validate the success of the process of reactivation of the Tonatzintla Schmidt Camera. From the light curve analyses, we noticed that even those with larger errors reproduce with very good agreement the periods previously determined by other authors. For each of the objects in our sample, we compared the best fit value of the period with those values on the summary line on LCDB, considered the most likely to be correct, and we found that the difference between them and ours was always less than 3%, and very often less than 1%.

There is one exception, (25916) 2001 CP44, which has two clearly distinct sets of values for its reported periods, one of them is equal, within the error bars, to the best value we found from our data; however, for the second one the difference is larger. As we mentioned, the difference can be due to observations being made during different apparitions.

In subsequent papers we will discuss these results as part of a larger sample of asteroids that we have already observed. We will present the analyses of the observations, including other results such as the determination of their morphological properties.

In concluding, we want to remark that the Tonantzintla Schmidt Camera is now dedicated to astrometric and photometric follow-up observations of Main Belt and Near-Earth Asteroids. It is a fundamental part of the asteroid observation program to fulfill the commitments made by INAOE and CRECTEALC regarding their contributions to the International Asteroid Warning Network (IAWN).

The authors would like to acknowledge the telescope technicians A. Marquez and C. Escamilla for their help during the observations and during the whole reactivation process of the CST, as well as J. Alva†, the INAOE engineer expert on the CST; without his historical knowledge it would have been very difficult to reactivate the telescope. We also want to thank L. Altamirano and D. Sánchez de la Llave, former INAOE General Director and former INAOE Research Director, respectively, and J. Moctezuma, A. Tuxpan, J. Escobar and P. García-Flores, members of the INAOE Computer Vision Lab.

REFERENCES

Alí-Lagoa, V. & Delbo', M. 2017, A&A, 603, 55, https://doi.org/10.1051/0004-6361/201629917

Binzel, R. P., DeMeo, F. E., Turtelboom, E. V., et al. 2019, Icar, 324, 41, https://doi.org/10.1016/j.icarus.2018.12.035

Bus, S. J. & Binzel, R. P. 2002, Icar, 158, 146, https://doi.org/10.1006/icar.2002.6856

Cardona, O., Carramiñana, A., Carrasco, E., & Escamilla, C. 2011, Nuevo Sistema de Adquisición de Imágenes Astronómicas de la Cámara Schmidt utilizando un CCD Enfriado. Reporte Técnico de la Coordinación de Astrofíisica, INAOE. http://inaoe.repositorioinstitucional.mx/jspui/handle/1009/911

Chang, C.-K., Ip, W.-H., Lin, H.-W., et al. 2015, ApJS, 219, 27, https://doi.org/10.1088/0067-0049/219/2/27

Díaz-Hernández, R., González, J. J., Costero, R., & Guichard, J. 2011, Proc. SPIE8011, 2nd Congress of the International Commission for Optics: Light for the Development of the World, https://doi.org/10.1117/12.903386

Harris, A. W., Pravec, P., Galád, A., et al. 2014, Icar, 235, 55, https://doi.org/10.1016/j.icarus.2014.03.004

Harris, A. W., Young, J. W., Bowell, E., et al. 1989, Icar, 77, 171, https://doi.org/10.1016/0019-1035(89)90015-8

Jáuregui, J. M., Cardona, O., Escamilla, C., Castillo-Domínguez, E., & López-Cruz, O. 2014, Sistema de Control para la Cámara Schmidt de Tonantzintla. Reporte Técnico No. RT0612. Coordinación de Astrofísica, INAOE. http://inaoe.repositorioinstitucional.mx/jspui/handle/1009/1158

Kaasalainen, M., Pravec, P., Krugly, Y. N., et al. 2004, Icar, 167, 178, https://doi.org/10.1016/j.icarus.2003.09.012

Kaasalainen, M., Mottola, S., & Fulchignoni, M. 2002, Asteroids III, ed. W. F. Bottke Jr., A. Cellino, P. Paolicchi, and R. P. Binzel (Tuczon, AZ: UAP), 139

Kaasalainen, M. & Torppa, J. 2001, Icar, 153, 24, https://doi.org/10.1006/icar.2001.6673

Kaasalainen, M., Torppa, J., & Muinonen, K. 2001, Icar, 153, 37, https://doi.org/10.1006/icar.2001.6674

Kryszczyńska, A., Colas, F., Polińska, M., et al. 2012, A&A, 546, 72, https://doi.org/10.1051/0004-6361/201219199

Lin, C.-H., Ip, W.-H., Lin, Z.-Y., et al. 2018, Planet. Space Sci., 152, 116, https://doi.org/10.1016/j.pss.2017.12.019

Mainzer, A., Grav, T., Masiero, J., et al. 2011, ApJ, 741, 90, https://doi.org/10.1088/0004-637X/741/2/90

Mainzer, A. K., Bauer, J. M., Cutri, R. M., et al. 2016, NASA Planetary Data System, EAR-A-COMPIL-5-NEOWISEDIAM-V1.0

Malcolm, G. 2002, Minor Planet Bulletin, 29, 28

Masiero, J. R., Mainzer, A. K., Grav, T., et al. 2012, ApJ, 759, 8, https://doi.org/10.1088/2041-8205/759/1/L8

Minor Planet Circular 6210. 1981 Aug. 1

Nesvorny, D. 2015, NASA Planetary Data System, EAR-A-VARGBDET-5-NESVORNYFAM-V.3.0

Nesvorný, D., Brož, M., & Carruba, V. 2015, Asteroids IV, 297, https://doi.org/10.48550/arXiv.1502.01628

Nugent, C. R., Mainzer, A., Masiero, J., et al. 2015, ApJ, 814, 117, https://doi.org/10.1088/0004-637X/814/2/117

Nugent, C. R., Mainzer, A., Bauer, J., et al. 2016, AJ, 152, 63, https://doi.org/10.3847/0004-6256/152/3/63

Popescu, M., Licandro, J., Carvano, J. M., et al. 2018, A&A, 617, 12, https://doi.org/10.1051/0004-6361/201833023

Popescu, M., Vaduvescu, O., de León, J., et al. 2019, A&A, 627, 124, https://doi.org/10.1051/0004-6361/201935006

Pravec, P., Harris, A. W., Kušnirák, P., Galád, A., & Hornoch, K. 2012, Icar, 221, 365, https://doi.org/10.1016/j.icarus.2012.07.026

Pravec, P. & Harris, A. W. 2000, Icar, 148, 12, https://doi.org/10.1006/icar.2000.6482

Schmadel, L. 2012, Dictionary of Minor Planet Names (Berlin: Springer Berlin Heidelberg), https://doi.org/10.1007/978-3-642-29718-2

Tedesco, E. F., Noah, P. V., Noah, M., et al. 2004, NASA Planetary Data System, IRAS-A-FPA-3-RDR-IMPS-V6.0

Tholen, D. J. 1984, Asteroid Taxonomy from Cluster Analysis of Photometry, Ph.D. Thesis, The University of Arizona

Tholen, D. J. & Barucci, M. A. 1989, in Asteroids II (Tuczon, AZ: UAP), 298

Thomas, C. A., Emery, J. P., Trilling, D. E., et al. 2014, Icar, 228, 217, https://doi.org/10.1016/j.icarus.2013.10.004

Usui, F., Kuroda, D., Müller, T. G., et al. 2011, PASJ, 63, 1117, https://doi.org/10.1093/pasj/63.5.1117

Valdés, J. R., Márquez, A., Guichard, J., et al. 2015a, Procedimiento para retirar la celda y el espejo de la Cámara Schmidt de Tonantzintla. Reporte Técnico. Coordinación de Astrofísica. INAOE

Valdés, J. R, Márquez, A., Guichard, J., et al. 2015b, Procedimiento para la limpieza de la Lente Correctora de la Cámara Schmidt de Tonantzintla. Reporte Técnico. Coordinación de Astrofísica. INAOE

Vereš, P., Jedicke, R., Fitzsimmons, A., et al. 2015, Icar, 261, 34, https://doi.org/10.1016/j.icarus.2015.08.007

Warner, B. D., Harris, A. W., & Pravec, P. 2009, Icar, 202, 134, https://doi.org/10.1016/j.icarus.2009.02.003

Warner, B. D. 2014, MPO Software, MPO Canopus version 10.4.3.17. Bdw Publishing. http://www.minorplanetobserver.com/

Waszczak, A., Chang, C.-K., Ofek, E. O., et al. 2015, AJ, 150, 75, https://doi.org/10.1088/0004-6256/150/3/75

Wisniewski, W. Z., Michalowski, T. M., Harris, A. W., & McMillan, R. S. 1995, Abstracts of the Lunar and Planetary Science Conference, 26, 1511

Wolfschmidt, G. 2009, AN, 330, 555, https://doi.org/10.1002/asna.200911216

S. Camacho and J. Guichard: Centro Regional de Enseñanza de Ciencia y Tecnología del Espacio para América Latina y el Caribe (CRECTEALC), (jguich, sergio.camacho@inaoep.mx).

S. Camacho, G. Cerdán, J. Guichard, J. Michimani, R. Mújica, J. R. Valdés, and R. Vega: Instituto Nacional de Astrofísica, Óptica y Electrónica (INAOE). Luis Enrique Erro # 1, Tonantzintla, Puebla, México C.P. 72840, (sergio.camacho@inaoep.mx, guillermocerdanher@gmail.com, jguich, michimani, rmujica, jvaldes, rvega@inaoep.mx)